Electronic Supplementary Information (ESI†)

High-Areal-Capacity Conversion Type Iron-Based Hybrid Redox Flow Batteries

*Yang Shi, Zengyue Wang, Yanxin Yao, Wanwan Wang and Yi-Chun Lu**

Electrochemical Energy and Interfaces Laboratory, Department of Mechanical and Automation Engineering, The Chinese University of Hong Kong, Shatin, N.T. 999077, Hong Kong SAR, China

Corresponding Author Yi-Chun Lu*. E-mail: yichunlu@mae.cuhk.edu.hk

Experimental section

Materials

All chemicals were used as received without further purification. Potassium ferricyanide ($K_3Fe(CN)_6$, AR) and Potassium ferrocyanide ($K_4Fe(CN)_6$ $3H_2O$, AR) were purchased from Xilong Chemcial CO., LTD and Sigma-Aldrich, respectively. Potassium iodide (KI, ≥ 99%), potassium hydroxide (KOH, ≥ 85%), sulfuric acid (H_2SO_4, 95-98%), N-methyl pyrrolidone (NMP) were received from Sigma-Aldrich. Polyvinylidene difluoride (PVDF) and Ketjen black (KB) were received from MTI. Hydrogen peroxide (H_2O_2, 30wt% in H_2O) was received from Dieckmann, Shenzhen. Reduced carbonyl iron powder (Fe, 98%) was received from Aladdin, Shanghai. Carbon felts were received from Beijing Jinglong Special Carbon Technology Co., Ltd and SGL Carbon. Nafion membrane (N117) were received from Shanghai Hesen Electric Co., Ltd.

Synthesis of carbonyl iron-KB-Bi_2S_3 composite

The active iron composite powder was synthesized by a simple ball milling method. Briefly, the commercial carbonyl iron powder and KB carbon and Bi_2S_3 was first ball milled for 12 hours at 400 rpm with a mass ratio at 75:5:5 and materials to ball ratio at 1:30.

Preparation of conversion iron negative electrode

The conversion iron negative electrode was prepared by a similar method reported by our group[1]. Specifically, the as-obtained iron composite powder was further mixed with KB and PVDF in NMP (1 wt.%) with a mass ratio at 85:5:10 (active materials: KB: PVDF at 8:1:1) to form a slurry. Then, the slurry was sonicated for 20 min to obtain a uniform suspension and infiltrated into the carbon felt (~10 mg cm^{-2}, surface area is 0.08 m^2 g^{-1}) and dried at 80°C for 6 h in vacuum. The loading is determined by the amount of slurry used and calculated by weight difference of electrode and pristine carbon felt. For the cells with areal capacity <45 mAh cm^{-2}, one piece of as-fabricated electrode was used. For the cells with areal capacity <135 mAh cm^{-2}, three pieces of electrodes were laminated together to achieve the high mass loading. For the cells with areal capacity >200 mAh cm^{-2}, six pieces of electrodes were laminated together, and the cell gaskets were changed from 3 mm to 6 mm.

All the gravimetric capacities with unit in mAh g^{-1} were calculated based on the mass loading of the active iron metal (carbonyl iron powder).

Formation process of conversion iron negative electrodes

To activate the activity of the iron negative electrode and obtain an electrode with a starting state at Fe_3O_4, we developed an electrode formation process, which was conducted in a H-type cell (with Hg/HgO reference electrode in negative electrode side) or in a flow cell (without reference electrode). At the beginning stage of the formation, the metallic iron was first oxidized to $Fe(OH)_2$ and then to the final product Fe_3O_4. Next, the oxidation product Fe_3O_4 was reduced to $Fe(OH)_2$. After this process, theoretically

the $Fe(OH)_2$ would be further reduced to Fe, however, the severe hydrogen evolution side reaction competes with this reaction, only a small amount of $Fe(OH)_2$ were reduced to Fe, most of the capacities were used for water spilling to generate hydrogen, which is undesirable. With the oxidation and reduction reaction processing, metal Fe were gradually oxidized and then accumulated to $Fe(OH)_2$, the $Fe(OH)_2$ to Fe_3O_4 were gradually dominated in the whole process. The parasite hydrogen evolution reaction gradually disappeared; the coulombic efficiency of this process became higher than 99%. This formation process was clearly presented in Fig. S1. From the 1st cycle to the 40th cycle, The HER plateau around −1.2 V vs. Hg/HgO shortened gradually which implies that the HER reaction percentage decreased significantly after the 40-cycle formation process. The electrode after formation were used in flow batteries later.

Conversion type hybrid RFBs assembly

The structure of flow cell stack was shown in Fig. S2. The flow battery was assembled by sandwiching the ion exchange membrane (Nafion 117 or Fumasep E620K or charge-reinforced ion-selective (CRIS) membrane) with positive electrode (SGL carbon felts) and negative electrode (conversion iron electrode) and clamped by two bipolar plates with parallel flow channel and further fixed by two stainless steel plates and crews. The excess posolyte is composed by 0.4 M potassium ferrocyanide ($K_4Fe(CN)_6$) in 1 M potassium hydroxide (KOH). The negolyte is composed by 3 M KOH and 1 M LiOH. The addition of Li ion in negolyte is used to prevent passivation of iron negative electrodes.[2] For cells with areal capacity <45 mAh cm^{-2}, 10 mL negolyte were used; for the cells with areal capacity <135 mAh cm^{-2}, 25 mL negolyte were used; for the cells with areal capacity >200 mAh cm^{-2}, 50 mL negolyte were used. The effective area of the electrode was 4 cm^2 (2 cm × 2 cm). The electrolytes were pumped by peristaltic pumps (Kamoer) with flow rate at 50-60 mL min^{-1}, or diaphragm pumps (Kamoer) with flow rate at 80-100 mL min^{-1} (only for iodine related cells).

Electrochemical measurements

Cyclic voltammetry (CV) was conducted in a three-electrode beaker cell with conversion iron electrode as working electrode, a platinum plate (1 cm × 1 cm) as the counter electrode and a Hg/HgO as a reference electrode (Hg/HgO in 1 M KOH solution. Shanghai Chuxi Industrial Co. Ltd.), solution of 3 M KOH and 1 M LiOH as electrolyte with a VMP3 electrochemical testing unit (Bio-Logic, France). Galvanostatic discharge/charge tests were performed on a LAND CT2001A battery test system (Wuhan LAND electronics Co., Ltd, China) and a VMP3 electrochemical testing unit (Bio-Logic, France). The upper limit of the charging process was limited by the gravimetric capacity of active iron metal (300 mAh g^{-1}, 94% of the theoretical capacity 319 mAh g^{-1}). All volumetric capacities and areal capacities are calculated based on the negative electrode side. Electrochemical impedance spectroscopy (EIS) measurements were performed by using the Bio-Logic or Arbin MSTAT21044 testing unit (Arbin Instruments Corp., USA) with the frequency range of 1 MHz to 0.1 Hz at an amplitude of 10 mV.

Material characterizations

Field emission scanning electron microscopy (SEM) was performed using a JSM-7800F (JEOL, Japan) with a sputtered conductive coating. X-Ray diffraction (XRD) was conducted with a Rigaku Smartlab diffractometer (Cu Kα radiation). The electrode samples were sealed in a glass sample holder with Kapton tape in glove box to avoid the sample degradation caused by ambient environment. The UV-visible (UV-vis) spectra were collected by SEC2000 UV-visible Spectrophotometer (ALS. Co., Ltd.).

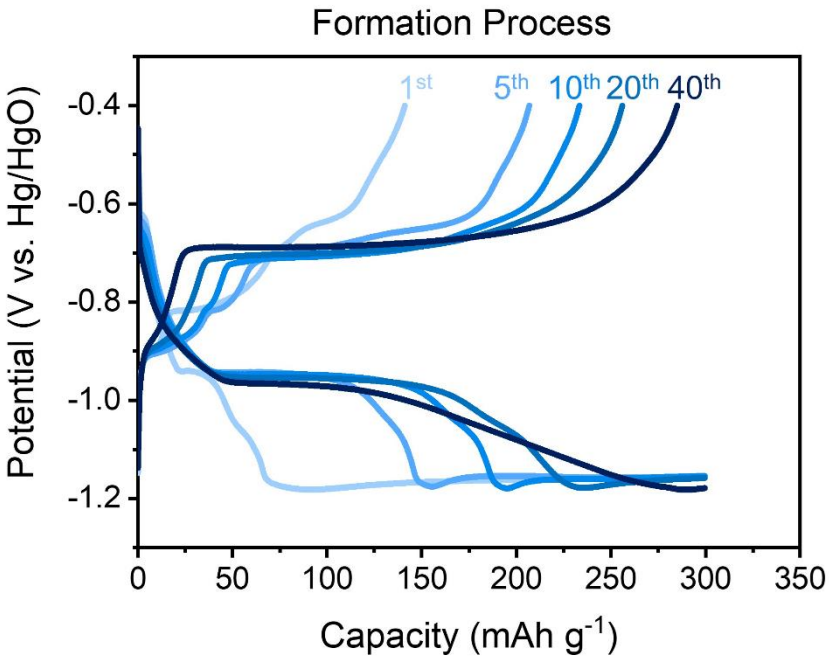

Fig. S1. The formation process of a conversion iron negative electrode with areal loading at 20.8 mg cm^{-2}. The current density was 300 mA g^{-1} and 6.23 mA cm^{-2}. The formation process was performed in a H-type cell with three-electrode setup. The reference electrode was Hg/HgO and the counter electrode was carbon felt with excess posolyte consisted of 0.4 M $K_4Fe(CN)_6$ in 1 M KOH in the other side separated by Nafion 117 membrane. The negolyte is 10 mL 3 M KOH and 1 M LiOH.

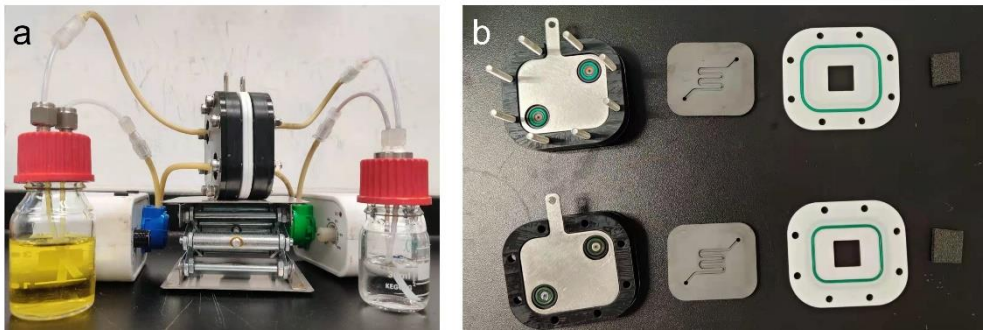

Fig. S2. (a) Digital image of flow battery device; (b) Digital image of the flow battery cell components.

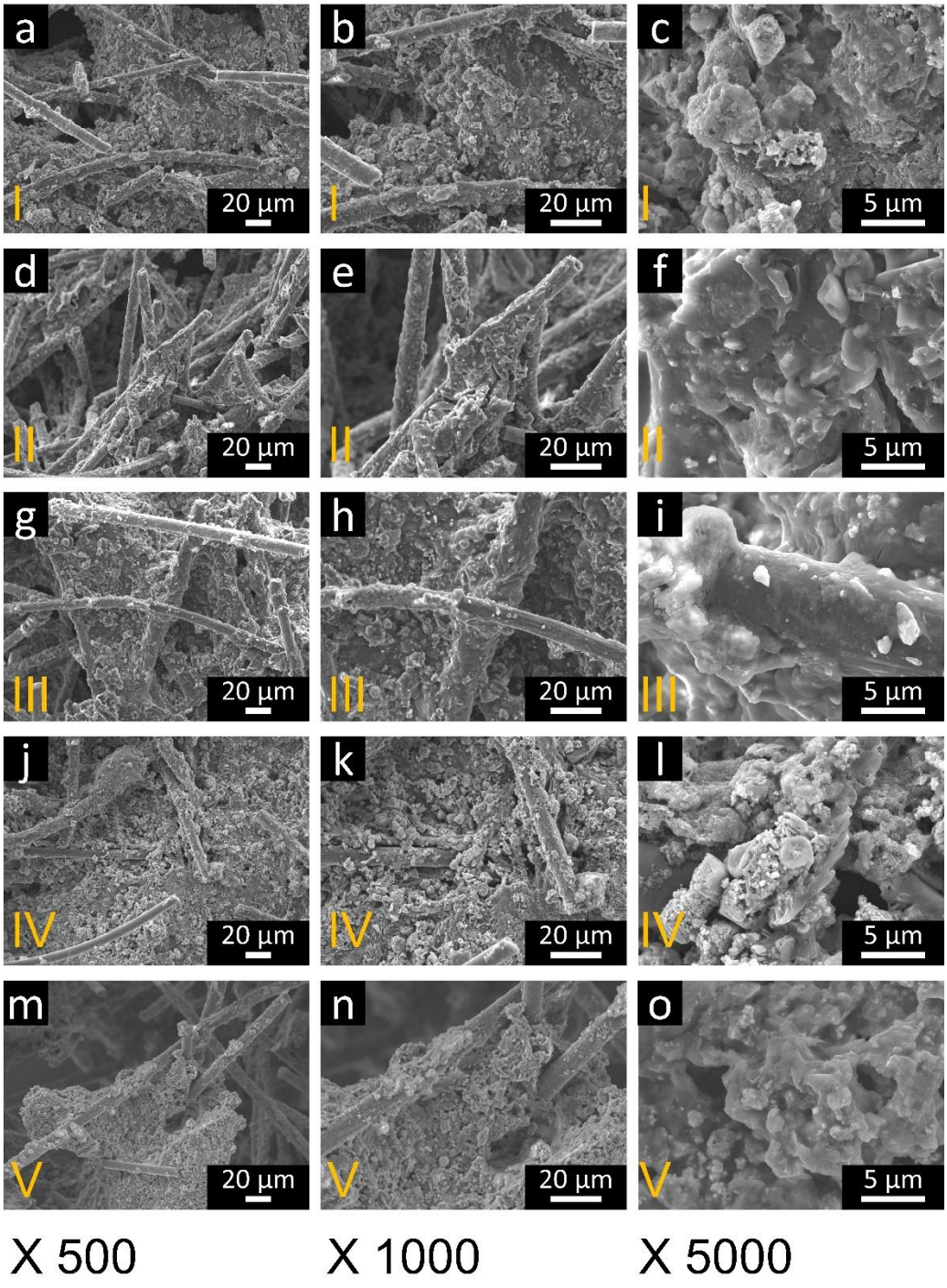

Fig. S3. The SEM images of the conversion iron negative electrode with different magnifications at state I to V; accordingly, (a)-(c) stage I; (d)-(f) stage II; (g)-(i) stage III; (j)-(l) stage IV; (m)-(o) stage V.

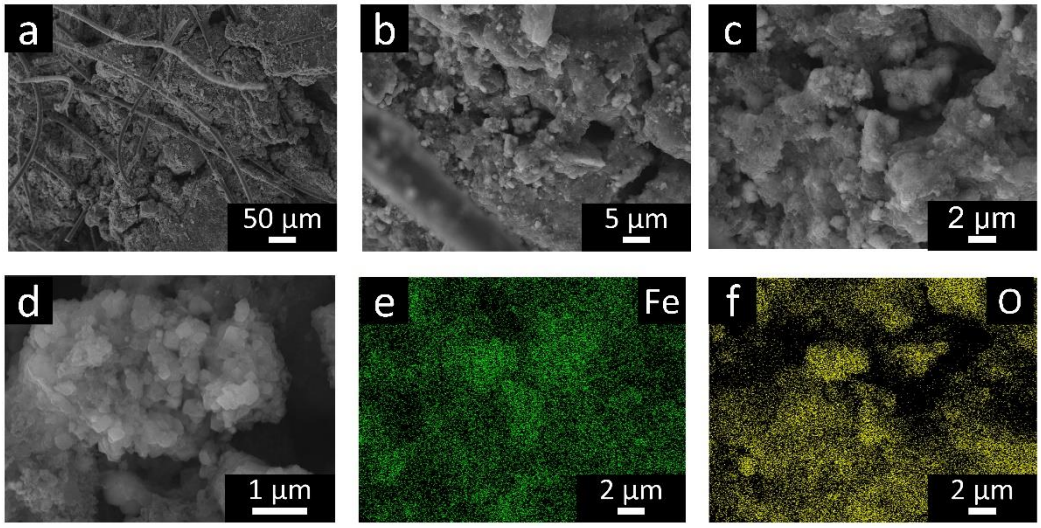

Fig. S4. The SEM images of the conversion iron negative electrode after formation process. (a) 200 magnifications; (b) 2000 magnifications; (c) 5000 magnifications; (d) 20000 magnifications; (e)-(f) the EDX mapping of (c): (e) Fe element; (f) O element.

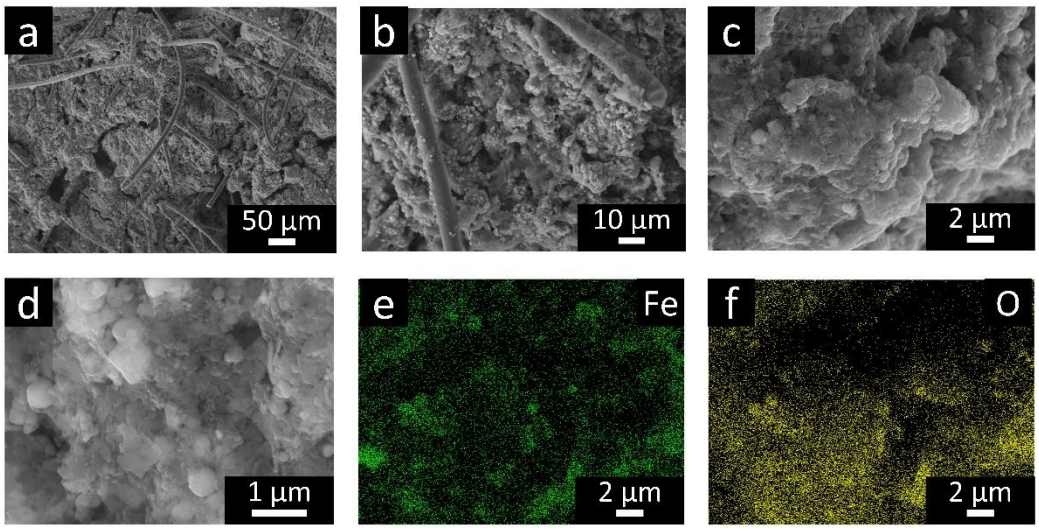

Fig. S5. The SEM images of the conversion iron negative electrode after 600 cycles with areal capacity of 25 mAh cm^{-2} and current density of 80 mA cm^{-2}. (a) 200 magnifications; (b) 1000 magnifications; (c) 5000 magnifications; (d) 20000 magnifications; (e)-(f) the EDX mapping of (c): (e) Fe element; (f) O element.

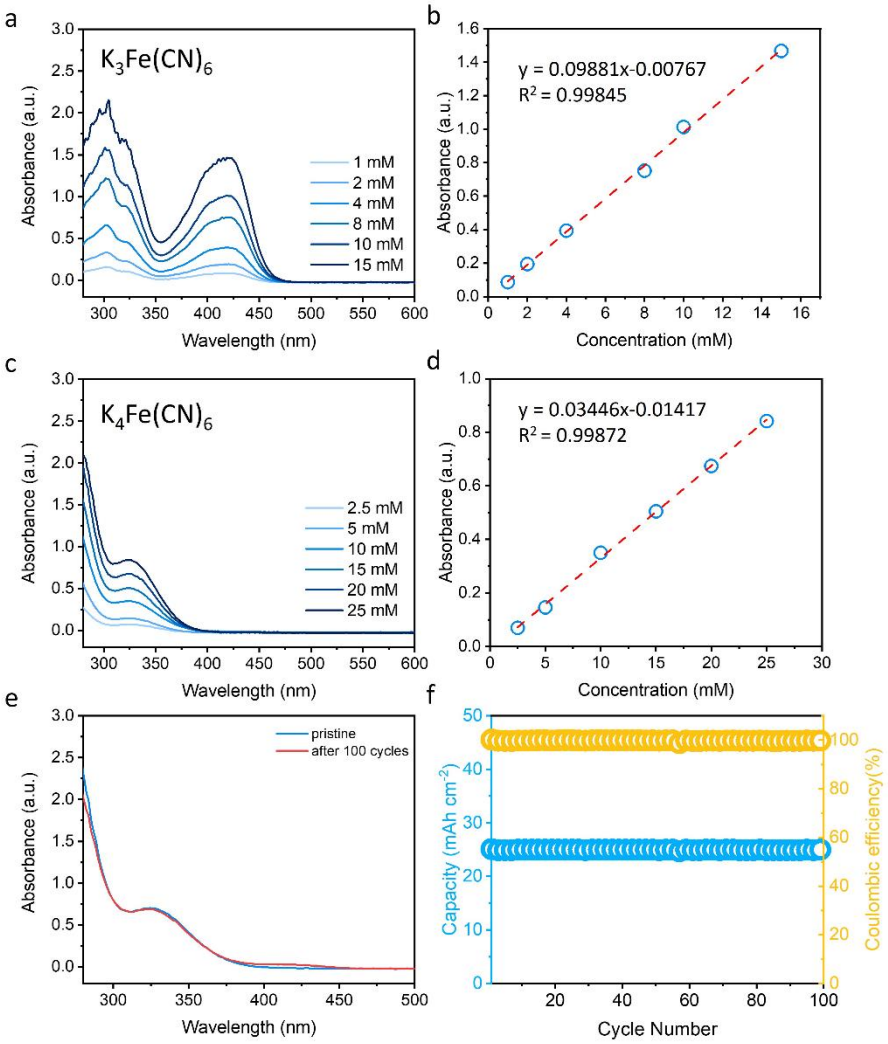

g

Concentration	$K_4Fe(CN)_6$ (mM)	$K_3Fe(CN)_6$ (mM)	Total (mM)	Before Dilution (mM)
pristine	20.72562	0.006442	20.732062	414.64124
after 100 cycles	20.35194	0.361704	20.713644	414.27288

Fig. S6. (a)-(b) UV-Vis spectra (a) of $K_3Fe(CN)_6$ with different concentration in 1 M KOH and the corresponding calibration plots (b) based on maximal absorption at 419.06 nm; (c)-(d) UV-Vis spectra (c) of $K_4Fe(CN)_6$ with different concentration in 1 M KOH and the corresponding calibration plots (d) based on maximal absorption at 326.42 nm; (e) UV-Vis spectra of posolyte (diluted 20 times by 1 M KOH) before (blue) and after (red) 100 galvanostatic cycles; (f) Cycling retention of areal capacity and coulombic efficiency of the conversion all-iron hybrid RFB (conversion iron electrode with 10 mL 3 M KOH 1 M LiOH // 20 mL 0.4 M $K_4Fe(CN)_6$ in 1 M KOH) at 80 mA cm^{-2} for 100 mAh; (g) Concentration of posolyte before and after 100 cycles calculated according to the calibration plots.

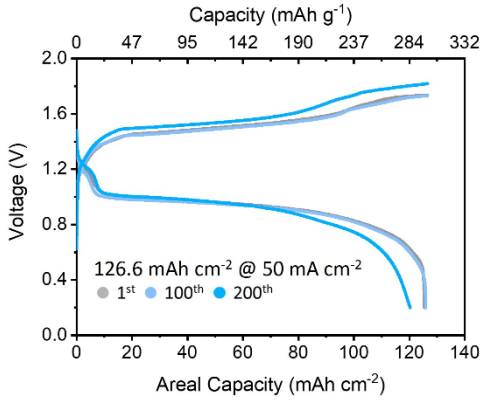

Fig. S7. Galvanostatic voltage profiles of the conversion all-iron hybrid RFB with a high loading negative electrode (126.6 mAh cm^{-2}) at a current density of 50 mA cm^{-2}.

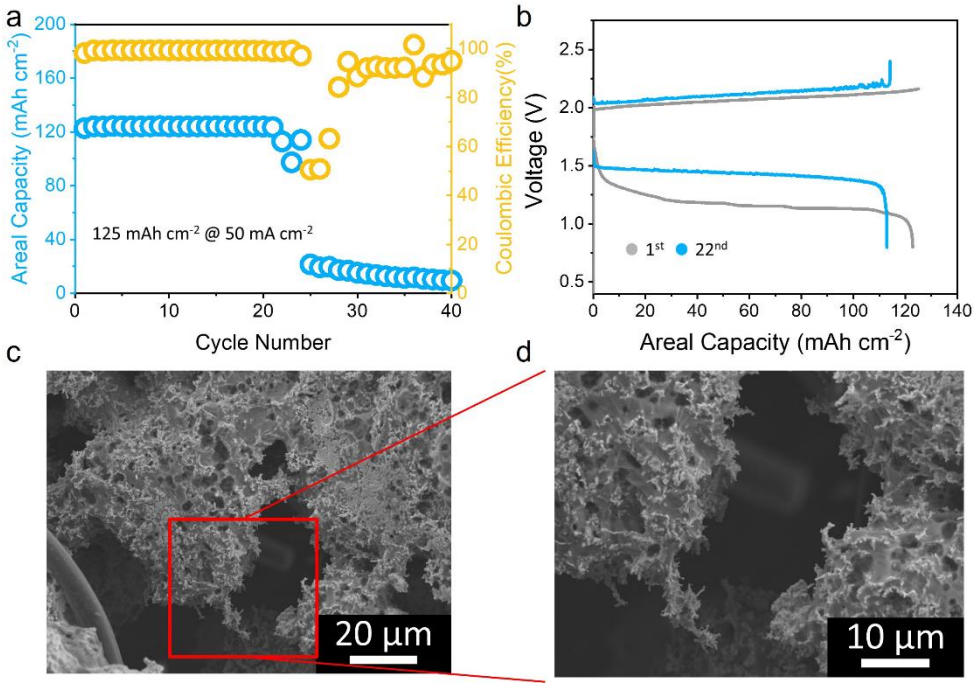

Fig. S8. Performance of the alkaline Zn-ferrocyanide flow battery with areal capacity of 125 mAh cm^{-2} and current density of 50 mA cm^{-2}. (a) cycling stability of the alkaline Zn-ferrocyanide flow battery; (b) Galvanostatic voltage profiles; (c) SEM image of Zn negative electrode at 1000 magnifications; (d) SEM image of Zn negative electrode at 2000 magnifications.

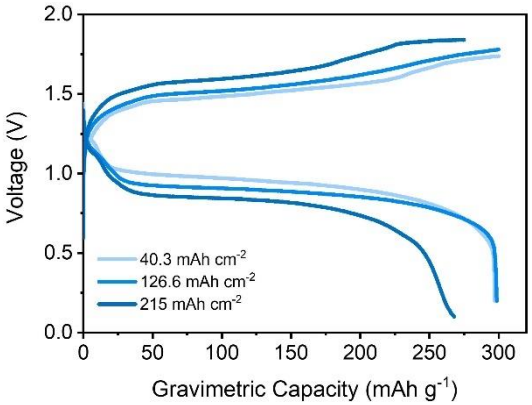

Fig. S9. Gravimetric capacity of conversion iron negative electrodes with different loading.

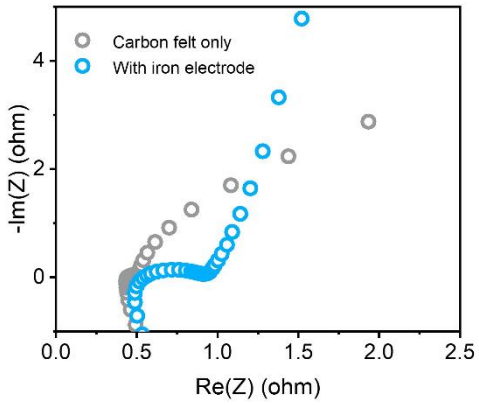

Fig. S10. EIS comparison of flow cell using conversion iron negative electrode on carbon felt and carbon felt only.

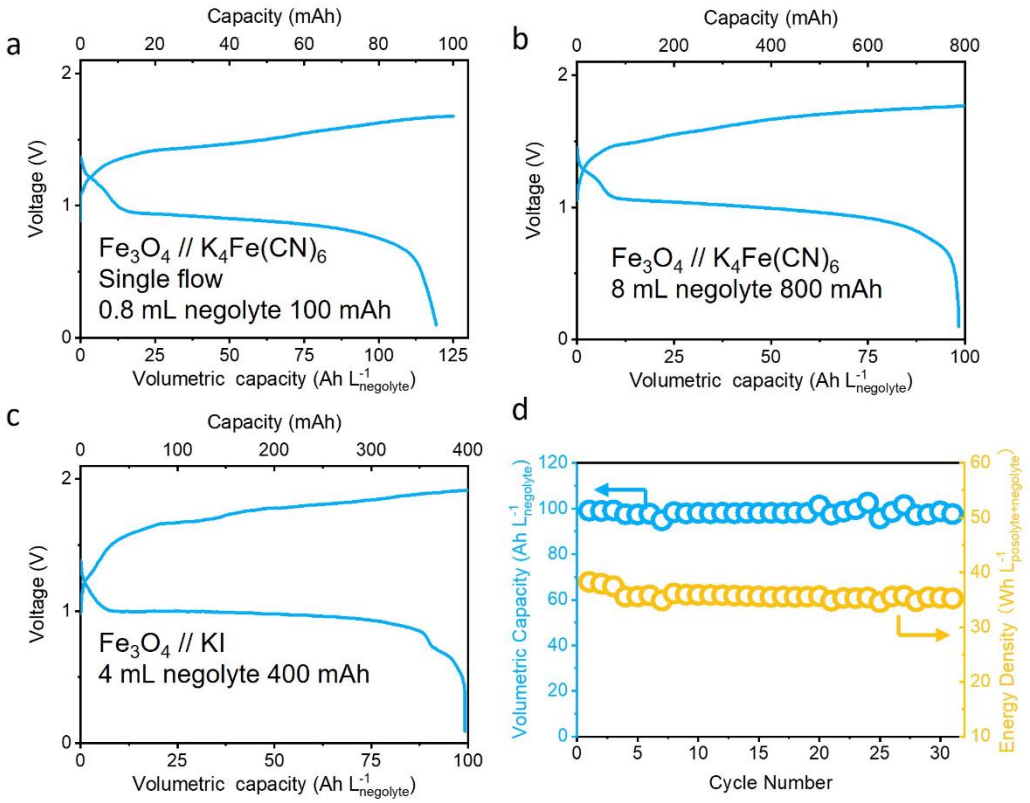

Fig. S11. (a) Representative galvanostatic voltage profile of the conversion all-iron hybrid RFB (conversion iron electrode with 0.8 mL 6 M KOH 1 M LiOH // 15 mL 0.4 M $K_4Fe(CN)_6$ in 1 M KOH) with static negolyte at 50 mA cm^{-2} for 100 mAh; (b) Representative galvanostatic voltage profile of the conversion all-iron hybrid RFB (conversion iron electrode with 8 mL 6 M KOH 1 M LiOH // 100 mL 0.4 M $K_4Fe(CN)_6$ in 1 M KOH) at 50 mA cm^{-2} for 800 mAh; (c)-(d) Galvanostatic voltage profile (c) and long-term cycling stability (d) of the conversion type iron-iodine hybrid RFB (conversion iron electrode with 4 mL 6 M KOH 1 M LiOH // 6 mL 4 M KI) at 20 mA cm^{-2} for 400 mAh with CRIS membrane.

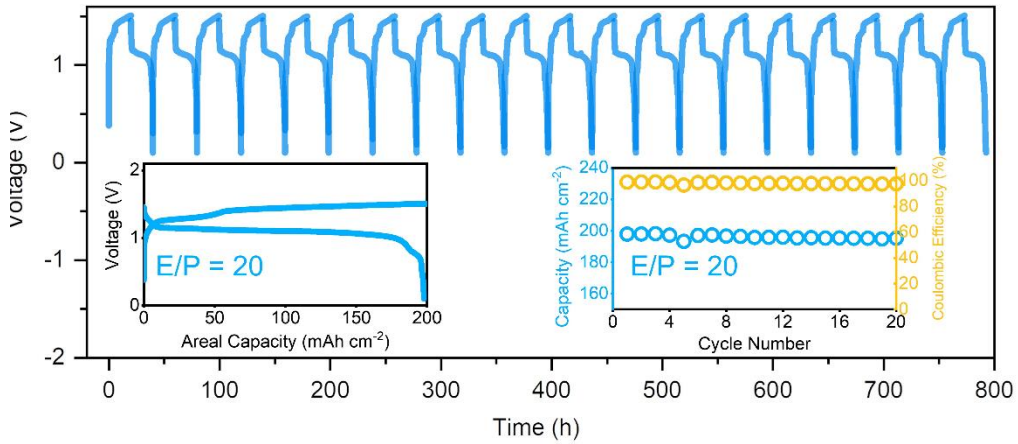

Fig. S12. Long discharge duration cycling of the conversion all-iron hybrid RFB (conversion iron electrode with 50 mL 3 M KOH 1 M LiOH // 120 mL 0.4 M $K_4Fe(CN)_6$ in 1 M KOH) with an E/P ratio of 20 (10 mA cm^{-2} 200 mAh cm^{-2}), insert: representative voltage profile; CE and capacity retention over 800 hours of cycling.

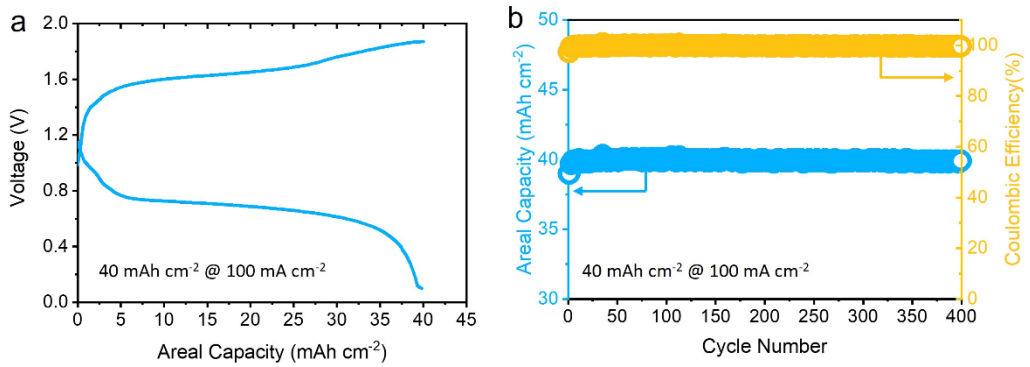

Fig. S13. (a)-(b) Representative galvanostatic voltage profiles (a) and long-term cycling stability (b) of conversion all-iron hybrid RFB (conversion iron electrode with 10 mL 3 M KOH 1 M LiOH // 25 mL 0.4 M $K_4Fe(CN)_6$ in 1 M KOH) at 40 mAh cm^{-2} and 100 mA cm^{-2}.

Table S1. Summary of state-of-art hybrid RFBs.

System	Current density (mA cm^{-2})	Areal Capacity (mAh cm^{-2})	Cycle number	Reference
Zn-I	10	22.5	50	3
	20	27.95	100	4
	80	23.18	500	
	40	204[a)]	80	5
Zn-Br	40	40	140	6
	100	20	5000	7
Zn-Fe	40	25	100	8
	100	26.25	210	9
Zn-Mn	40	13.3	100	10
Conversion All-Fe	80	25	600	This work
	100	40	400	
	50	126.6	200	
	60	215	100	

a) Estimated by coulombic efficiency and areal charge capacity.

Table S2. Detail information of cells reported in this paper.

Cell	Iron electrode volume	Negolyte	Membrane	Posolyte	Volume ratio of solid electrode to posolyte
Fig. 4	1.2 cm^3	10 mL 3 M KOH 1 M LiOH	N117	15 mL 0.4 M $K_4Fe(CN)_6$ in 1 M KOH	0.08
Fig. 5a	1.2 cm^3	25 mL 3 M KOH 1 M LiOH	N117	60 mL 0.4 M $K_4Fe(CN)_6$ in 1 M KOH	0.02
Fig. 5b	2.4 cm^3	50 mL 3 M KOH 1 M LiOH	N117	120 mL 0.4 M $K_4Fe(CN)_6$ in 1 M KOH	0.02
Fig. 6a-b	1.2 cm^3	10 mL 3 M KOH 1 M LiOH	E620K	25 mL 0.4 M $K_4Fe(CN)_6$ in 1 M KOH	0.048
Fig. 6c-d	1.2 cm^3	10 mL 3 M KOH 1 M LiOH	CRIS	10 mL 4 M KI	0.06
Fig. S6	1.2 cm^3	10 mL 3 M KOH 1 M LiOH	N117	20 mL 0.4 M $K_4Fe(CN)_6$ in 1 M KOH	0.06
Fig. S11a	1.2 cm^3	0.8 mL 6 M KOH 1 M LiOH	N117	15 mL 0.4 M $K_4Fe(CN)_6$ in 1 M KOH	0.08
Fig. S11b	2.4 cm^3	8 mL 6 M KOH 1 M LiOH	N117	120 mL 0.4 M $K_4Fe(CN)_6$ in 1 M KOH	0.02
Fig. S11c-d	1.2 cm^3	4 mL 6 M KOH 1 M LiOH	CRIS	6 mL 4 M KI	0.2
Fig. S12	2.4 cm^3	50 mL 3 M KOH 1 M LiOH	N117	120 mL 0.4 M $K_4Fe(CN)_6$ in 1 M KOH	0.02
Fig. S13	1.2 cm^3	10 mL 3 M KOH 1 M LiOH	N117	25 mL 0.4 M $K_4Fe(CN)_6$ in 1 M KOH	0.048

Techno-economic analysis:

The installed cost of conversion type all-iron hybrid RFBs with Nafion 117 membrane, with E620K membrane and deposition zinc-iodide hybrid RFBs were calculated[11-13] using the following equation (1) and plotted in Fig. 7b.

$$C_{installed} = \left(\frac{C_{power} + C_{bop}}{t_d} + C_{energy}\right) \times \left(1 + f_{installed}\right) + \frac{C_{add}}{t_d} \quad (1)$$

The definitions of terms were list below:

Term	Definition
C_{power}	Cost of power including the cell stack cost
C_{energy}	Cost of energy, which is the combined cost of negolyte and posolyte.
C_{bop}	Balance-of-plant cost including the costs of accessories (heating/cooling equipment, state-of-charge and power managing electronics, and pumps, needed to run a flow battery system).
C_{add}	Additional cost such as sales, administration, depreciation, warranty, research and development, profit margin, etc.
$f_{installed}$	System installation cost adjustment factor
t_d	Storage duration (hour)

We considered US$ 202.5 kW^{-1} and US$ 87.5 kW^{-1}, and 20.5% for C_{bop} and C_{add}, and $f_{installed}$, respectively. [11-13]

Chemical cost calculation (C_{energy}). The chemical cost of storage (CCS) can be calculated from equation (2): [11-13]

$$C_{energy} = \frac{C_{chemical} + C_{tank}}{\varepsilon_{sys,d} \times \varepsilon_{q,rt} \times \varepsilon_{v,d}} \quad (2)$$

The definitions of terms were list below:

Term	Definition
$C_{chemical}$	Combined cost of chemicals used in the negolyte and posolyte
C_{tank}	Bulk tank price (0.15 $US\$\ L^{-1}$) normalized by the energy density ($kWh\ L^{-1}$)
$\varepsilon_{sys,d}$	System round trip efficiency taken as a constant of 0.94
$\varepsilon_{q,rt}$	Coulombic efficiency of system
$\varepsilon_{v,d}$	The discharge voltage divided by cell open circuit voltage.

Assuming a 1 Ah system, the chemical cost can be calculated based on equation. 3-5 [11-13]:

$$C_{chemical}\ (CCS)(US\$\ kWh^{-1}) = \frac{Cost\ of\ negolyte + Cost\ of\ posolyte}{OCV \times 1 \times 0.001} \quad (3)$$

For deposition hybrid RFBs[11-13]:

$$\text{Cost of negolyte (US\$)} = \left[P_a \times C_a + P_{a,s} \times C_{a,s}\right] \times \frac{1\ Ah}{Cap_a} \quad (4)$$

$$\text{Cost of posolyte (US\$)} = \left[P_c \times C_c + P_{c,s} \times C_{c,s}\right] \times \frac{1\ Ah}{Cap_c} \quad (5)$$

For conversion type hybrid RFBs[6]:

$$\text{Cost of negative electrode (US\$)} = \left[P_{a,s} \times C_{a,s}\right] \times \frac{1\ Ah}{Cap_{a,\ con}} + P_{a,con} \times \frac{1\ Ah}{Cap_{a,\ con}} \quad (6)$$

The definitions of terms were list below:

Term	Definition
P_a and P_c	Price $(US\$\ mol^{-1})$ of active material
C_a and C_c	Concentration $(mol\ L^{-1})$ of the active materials
$P_{a,s}$ and $P_{c,s}$	Cost $(US\$\ mol^{-1})$ of the supporting materials
$C_{a,s}$ and $C_{c,s}$	Concentration $(mol\ L^{-1})$ of supporting electrolyte
Cap_a and Cap_c	Capacity $(Ah\ L^{-1})$ at the given concentration
$P_{a,con}$ and $Cap_{a,\ con}$	Cost $(US\$\ kg^{-1})$ and the specific capacity $(Ah\ kg^{-1})$ of the solid negative electrode materials.

The bulk prices for chemicals are listed, and the chemical cost calculation details by using the above equations are presented in Table S3-S5.

Cost of power calculation (C_{power}). The power cost was calculated as follow[11-13]:

$$C_{power}\left(US\$\ kW^{-1}\right) = \frac{C_a}{\varepsilon_{sys,d} \times V_d \times I} \quad (7)$$

The definitions of terms were list below:

Term	Definition
C_a	Total cell stack component cost per unit area $(US\$\ m^{-2})$
V_d	The average discharge voltage of the cell (V)
I	Current density $(A\ m^{-2})$
$\varepsilon_{sys,d}$	System round trip efficiency

C_a depends on the cost of each stack component, as are represented in Table S6.

Table S3. Calculation of chemical cost of positive electrode.

Chemical cost of positive electrode					
	bulk price (US$ kg^{-1})	Concentration (mol L^{-1})	MW (kg mol^{-1})	Capacity (Ah L^{-1})	Cost (US$ Ah^{-1})
$K_4Fe(CN)_6$	2[14]	0.5	0.36835	13.4	0.027489
KOH	0.82[12]	1	0.05611		0.003434
Chemical Cost (US$ Ah^{-1})					0.030922

Table S4. Calculation of chemical cost of negative electrode.

Chemical cost of negative electrode				
	Bulk price (US$ kg^{-1})	MW (kg mol^{-1})	Capacity (Ah kg^{-1})	Cost (US$ Ah^{-1})
Fe	0.17[15]	0.056	300	0.000567
KOH	0.82[12]	0.05611		0.002054
LiOH H_2O	1.52[12]	0.042		0.002850
Chemical Cost (US$ Ah^{-1})				0.005471

Table S5. Calculation of energy cost.

System	Cost of positive electrode (US$ Ah^{-1})	Cost of negative electrode (US$ Ah^{-1})	OCV (V)	$C_{chemical}$ (US$ kWh^{-1})	C_{tank} (US$ kWh^{-1})	ε_{sys} (%)	$\varepsilon_{q,rt}$ (%)	$\varepsilon_{v,d}$ (%)	C_{energy} (US$ kWh^{-1})
All-Fe @ N117	0.030922	0.005471	1.16	31.373359	11.58003	0.94	0.99	0.81	56.983534
All-Fe @ E620K	0.030922	0.005471	1.16	31.373359	11.58003	0.94	0.99	0.83	55.610436

Table S6. Calculation of power cost.

System	Membrane (US$ m^{-2})	GF (US$ m^{-2})	Frames (US$ m^{-2})	Stainless steel (US$ m^{-2})	$C_{cell\ stack}$ (US$ m^{-2})	I (A m^{-2})	V_d (V)	C_{power} (US$ kW^{-1})
All-Fe @ N117	500[13]	4.14[12, 13]	2[12, 13]	5.9[12, 13]	522.08[12, 13]	500	0.95	1169.272116
All-Fe @ E620K	25[14]	4.14[12, 13]	2[12, 13]	5.9[12, 13]	47.08[12, 13]	500	0.96	104.343972

Table S7. Calculation of installed cost.

	Power Cost (US$ kW^{-1})	BOP Cost (US$ kW^{-1})	Energy Cost (US$ kWh^{-1})	Additional Cost (US$ kW^{-1})	$f_{installed}$
All-Fe @ N117	1169.272116	202.5	56.983534	87.5	0.205
All-Fe @ 620K	104.343972	202.5	55.610436	87.5	0.205
ZIFB[13]	1157.092199	202.5	734.91	87.5	0.205
VRFB[11, 12]	85	260	162	125	0.205

REFERENCES

1. Y. Zhou, Z. Wang and Y.-C. Lu, *Mater. Today Energy*, 2020, 100570.
2. K. Vijayamohanan, T. S. Balasubramanian and A. K. Shukla, *J. Power Sources*, 1991, **34**, 269-285.
3. G. M. Weng, Z. J. Li, G. T. Cong, Y. C. Zhou and Y. C. Lu, *Energy Environ. Sci.*, 2017, **10**, 735-741.
4. C. X. Xie, Y. Liu, W. J. Lu, H. M. Zhang and X. F. Li, *Energy Environ. Sci.*, 2019, **12**, 1834-1839.
5. S. Wang, C. Yuan, N. Chang, Y. Song, H. Zhang, Y. Yin and X. Li, *Sci. Bull.*, 2021, **66**, 889-896.
6. Y. Yin, S. Wang, Q. Zhang, Y. Song, N. Chang, Y. Pan, H. Zhang and X. Li, *Adv. Mater.*, 2020, **32**, e1906803.
7. J. H. Lee, R. Kim, S. Kim, J. Heo, H. Kwon, J. H. Yang and H. T. Kim, *Energy Environ. Sci.*, 2020, **13**, 2839-2848.
8. C. Xie, Y. Duan, W. Xu, H. Zhang and X. Li, *Angew. Chem. Int. Ed.*, 2017, **56**, 14953-14957.
9. Z. Yuan, Y. Duan, T. Liu, H. Zhang and X. Li, *iScience*, 2018, **3**, 40-49.
10. C. X. Xie, T. Y. Li, C. Z. Deng, Y. Song, H. M. Zhang and X. F. Li, *Energy Environ. Sci.*, 2020, **13**, 135-143.
11. R. M. Darling, K. G. Gallagher, J. A. Kowalski, S. Ha and F. R. Brushett, *Energy Environ. Sci.*, 2014, **7**, 3459-3477.
12. Z. Li, M. S. Pan, L. Su, P. C. Tsai, A. F. Badel, J. M. Valle, S. L. Eiler, K. Xiang, F. R. Brushett and Y. M. Chiang, *Joule*, 2017, **1**, 306-327.
13. M. Mousavi, G. Jiang, J. Zhang, A. G. Kashkooli, H. Dou, C. J. Silva, Z. P. Cano, Y. Niu, A. Yu and Z. Chen, *Energy Storage Mater.*, 2020, **32**, 465-476.
14. X. Wei, G.-G. Xia, B. Kirby, E. Thomsen, B. Li, Z. Nie, G. G. Graff, J. Liu, V. Sprenkle and W. Wang, *J. Electrochem. Soc.*, 2015, **163**, A5150.
15. Gold supplier with high transaction level from www.alibaba.com., https://www.alibaba.com, (accessed 08/04, 2021).